Journal of Solid State Chemistry 184 (2011) 1070–1078

Contents lists available at ScienceDirect

Journal of Solid State Chemistry

journal homepage: www.elsevier.com/locate/jssc

Polyoxometalate immobilization in Cu^{I}/Ag–pz porous coordination polymers: The influences of them on the structural properties of frameworks

Min Zhu, Jun Peng*, Hai-Jun Pang, Peng-Peng Zhang, Yuan Chen, Dan-Dan Wang, Ming-Guan Liu, Yong-Hui Wang

Key Laboratory of Polyoxometalate Science of Ministry of Education, Faculty of Chemistry, Northeast Normal University, Changchun, Jilin 130024, PR China

ARTICLE INFO

Article history:
Received 8 December 2010
Received in revised form
9 March 2011
Accepted 14 March 2011
Available online 21 March 2011

Keywords:
Porous coordination polymers
Keggin polyoxometalate templates
Photocatalytic activity
Photoluminescence and electrochemistry properties

ABSTRACT

Three new high dimensional Cu^{I}/Ag–pz porous coordination polymers (PCPs) with different Keggin polyoxometalate templates have been hydrothermally synthesized: $[Cu^{I}_5(pz)_6Cl][HPMo^{VI}_{10}Mo^{V}_2O_{40}]$ **(1)** $[Ag_5(pz)_7(BW_{12}O_{40})]$ **(2)** and $[Cu^{I}_5(pz)_6H(H_2W_{12}O_{40})]\cdot 4H_2O$ **(3)** (pz=pyrazine). The choice of the particular Keggin POM templates is shown to influence the structural properties of the Cu/Ag PCPs. Compound **1** shows a Cl-bridged Cu–pz–Cl double layer, between which two kinds of $[HPMo^{VI}_{10}Mo^{V}_2O_{40}]^{4-}$ (PMo_{12}) polyanions are located. Compound **2** presents a 3D Ag–pz framework with parallelogram-like voids, into which $BW_{12}O^{5-}_{40}$ (BW_{12}) Keggin ions are incorporated. Compound **3** contains a Cu–pz cationic layer framework, between which are located $[H(H_2W_{12}O_{40})]^{5-}$ (W_{12}) Keggin ions. Primary photocatalytic experiment indicates that compound **1** presents excellent photocatalytic activity. The photoluminescence properties and electrochemistry properties of the compounds are also discussed.

1. Introduction

Polyoxometalates (POMs), as metal-oxygen cluster species, are garnering increasing attention owing to their unmatched structural variety and diversity in composition, sizes and shapes, which endow them with numerous applications, such as acid and photo-oxidation catalysts, electronic sensors, molecular conductors, single molecule magnets, ferroelectric response, photochromic response and other optical activities [1–10]. However, their intrinsic drawbacks, including low specific surface area, low stability under catalytic conditions and high solubility in aqueous solution, frequently limit their applications. Many strategies to optimize their applications have been investigated in an effort. Among them, the most effective strategy is to immobilize POMs on various porous solid supports [11–18]. Recently, porous coordination polymers (PCPs), constructed from metal cations and bridging multitopic ligands, have been paid intensive attention as a new type of porous material with various appealing applications [19–26]. In particular, designing porous coordination polymers in the presence of templates is a promising and frontline area of research [27–29]. Stimulated by it, immobilizing POMs by enwrapping them in the nanosized voids of PCPs become a promising approach to optimize and improve the functionalities of POM materials by taking advantage of the high stability, high surface area and low solubility of PCPs [1,30–31].

Since the beginning of this area, POM-immobilized coordination polymers have been of great interest for crystal chemists [32–37]. In the last several years, many interesting POM-immobilized PCPs have been synthesized, in which N-donor containing PCPs range from metal-pyridyl polymers to metal-triazole clusters with the N-donor sites increased [38–42]. Both the PCPs and POMs contribute significantly to final structures of these polymers. On the one hand, PCPs can only stabilize nanosized POM whose size is analogous to the voids. On the other hand, POMs, as templates, can influence the structures of PCPs and regulate PCPs to accommodate themselves. Such synergistic interactions between POMs and PCPs are interesting and sensitive. Our previous work has demonstrated the influences of molar ratio of ligand to metal, template role of different polyoxovanadates and synergistic interactions among POMs, metal ions and flexible ligands on the structures in such system [43–44].

Pyrazine (pz), as a kind of small rigid ligand, often exhibits the linear bridging coordination mode to combine various transition metal cations [45–50]. Compared with the long flexible ligands, such as bbi, bix and so on, pz molecule has the advantage over them to construct porous rather than entangleable frameworks. In addition, its small steric hindrance may spare more space to accommodate the POM templates with large size. Thus, it may be a sound candidate for the design and synthesis of POM-templated coordination frameworks. Further, the metal-pyrazine complexes may serve as sensitizers under light irritation to promote electron

* Corresponding author.
E-mail addresses: jpeng@nenu.edu.cn, pjun56@yahoo.com, tianax717@nenu.edu.cn (J. Peng).

0022-4596/$ - see front matter © 2011 Elsevier Inc. All rights reserved.
doi:10.1016/j.jssc.2011.03.030

transfer to POMs, which may bring some improved properties than native POMs. As a continuousness of our work, we choose Cu^{I}/Ag–pz PCPs and three different Keggin ions to experiment.

Herein, we employ PMo_{12}, BW_{12} and W_{12} Keggin ions as templates, three POM-immobilized PCPs have been obtained: $[Cu^{I}_5(pz)_6Cl][HPMo^{VI}_{10}Mo^{V}_2O_{40}]$ **(1)** $[Ag_5(pz)_7(BW_{12}O_{40})]$ **(2)** and $[Cu^{I}_5(pz)_6H(H_2W_{12}O_{40})]\cdot 4H_2O$ **(3)** (pz = pyrazine). The structural properties of the Cu/Ag PCPs are shown to be influenced by particular Keggin POMs. Further, compound **1** includes an uncommon Cl-bridged *M*–pzCl double layer. Compound **2** represents a unique 3D *M*–pz PCP which are templated by BW_{12} ions. Compound **3** shows a W_{12} Keggin POM-templated framework constituted by Cu–pz cationic layers. The influences of Keggin ions on the structures of the three compounds are also discussed in the paper.

2. Experimental

2.1. Materials and methods

All reagents for synthesis were purchased from commercial sources and used without further purification. Elemental analyses (C, H and N) were performed on a Perkin-Elmer 2400 CHN Elemental Analyzer. The IR spectra were obtained on an Alpha Centaurt FT/IR spectrometer with KBr pellet in the $400-4000\ cm^{-1}$ region. X-ray photoelectron spectroscopy (XPS) analyses were performed on a VG ESCALAB MK II spectrometer with an Mg*K*α (1253.6 eV) achromatic X-ray source. The vacuum inside the analysis chamber was maintained at 6.2×10^{-6} Pa during analysis. The TG analyses were performed on a DTG-60AH instrument in flowing N_2 with a heating rate of 10 °C/min. The XRPD patterns were obtained with a Rigaku D/max 2500 V PC diffractometer with Cu–*K*α radiation, the scanning rate is 4°/s, 2θ ranging from 5° to 40°. Luminescence measurements were carried on a Hitachi F-4500 Fluorescence Spectrophotometer. UV–vis absorption spectra were recorded on a 756 CRT UV–vis spectrophotometer. Cyclic voltammograms were obtained with a CHI 660 electrochemical workstation at room temperature. Platinum gauze was used as a counter electrode and Ag/AgCl electrode was referenced. Chemically bulk-modified carbon paste electrodes (CPEs) were used as working electrodes.

2.2. Syntheses

2.2.1. Synthesis of $[Cu^{I}_5(pz)_6Cl][HPMo^{VI}_{10}Mo^{V}_2O_{40}]$ (**1**)

A mixture of $Na_2MoO_4\cdot 2H_2O$ (0.48 g, 1.98 mmol), H_3PO_4 (1 mL, 7.96 mmol), $CuCl_2\cdot 2H_2O$ (0.23 g, 1.35 mmol), pz (0.07 g, 0.87 mmol) and H_2O (10 mL) was stirred for an hour. The pH was adjusted to 2.6 with 2 M HCl, then sealed in an 18 mL Teflon-lined reactor and heated at 160 °C for 3 days. After the reactor was slowly cooled to room temperature over a period of 10 °C/h, black block crystals were filtered, washed with water, and dried at room temperature (yield 56%, based on Mo). $C_{24}H_{25}ClCu_5N_{12}O_{40}PMo_{12}$ (2656.94): Calc: C, 10.85%; H, 0.94%; N, 6.33%. Found: C, 10.26%; H, 1.09%; N, 6.15%. IR (solid KBr pellet, cm^{-1}): 3440 (w), 3250 (w), 3080 (w), 2920 (w), 1610 (w), 1420 (s), 1160 (m), 953 (s), 866(w), 779 (s), 669 (w).

2.2.2. Synthesis of $[Ag_5(pz)_7(BW_{12}O_{40})]$ (**2**)

A mixture of $Na_2WO_4\cdot 2H_2O$ (0.93 g, 2.82 mmol), H_3BO_3 (0.2 g, 3.23 mmol), $AgNO_3$ (0.15 g, 0.88 mmol), pz (0.11 g, 1.37 mmol) and H_2O (10 mL) was stirred for an hour. The pH was adjusted to 2.3 – 3.2 with 2 M HNO_3, then sealed in an 18 mL Teflon-lined reactor and heated at 160 °C for 3 days. After the reactor was slowly cooled to room temperature over a period of 10 °C/h, light-green block crystals were filtered, washed with water, and dried at room temperature (yield 62%, based on W). $C_{28}H_{28}Ag_5N_{14}O_{40}BW_{12}$ (3956.82): Calc: C, 8.50%; H, 0.71%; N, 4.96%. Found: C, 9.26%; H, 0.89%; N, 4.25%. IR (solid KBr pellet, cm^{-1}): 3440 (s), 3100 (w), 3040 (w), 1620 (w), 1420 (s), 1340 (w), 1160 (s), 1120 (m), 1050 (s), 995 (w), 943(s), 889 (s), 822 (s).

2.2.3. Synthesis of $[Cu^{I}_5(pz)_6H(H_2W_{12}O_{40})]\cdot 4H_2O$ (**3**)

A mixture of $Na_2WO_4\cdot 2H_2O$ (0.66 g, 2.00 mmol), $CuCl_2\cdot 2H_2O$ (0.19 g, 1.11 mmol), pz (0.08 g, 1 mmol) and H_2O (10 mL) was stirred for an hour. The pH was adjusted to 4.7 with 2 M HCl, then sealed in an 18 mL Teflon-lined reactor and heated at 160 °C for 3 days. After the reactor was slowly cooled to room temperature over a period of 10 °C/h, red block crystals were filtered, washed with water, and dried at room temperature (yield 59%, based on W). $C_{24}H_{27}Cu_5N_{12}O_{40}W_{12}$ (3647.34): Calc: C, 7.90%; H, 0.75%; N, 4.61%. Found: C, 7.26%; H, 0.89%; N, 4.65%. IR (solid KBr pellet, cm^{-1}): 3420 (s), 3080 (w), 3020 (w), 1610 (w), 1480 (m), 1410 (s), 1160 (s), 1110 (w), 991 (w), 947 (m), 883 (m), 798 (s), 675 (w).

2.3. Preparations of **1**, **2** and **3** – CPEs

Compound **1** – modified carbon paste electrode **1** – CPE was prepared as follows: 90 mg of graphite powder and 8 mg of compound **1** were mixed and ground together by agate mortar and pestle to achieve a uniform mixture, and then 0.6 mL nujol was added with stirring. The homogenized mixture was packed into a glass tube with 1.2 mm inner diameter, and the tube surface was wiped with paper. Electrical contact was established with copper rod through the back of the electrode. In a similar manner, **2**– and **3**–CPEs were made with compounds **2**–**3**.

2.4. X-ray crystallography

Crystal data for compounds **1**–**3** were collected on a Bruker SMART-CCD diffractometer, with Mo–*K*α monochromatic radiation (λ = 0.71069 Å) at 293 K. The structures were solved by the directed methods and refined by full matrix least-squares on F^2 using the SHELXTL crystallographic software package [51–52]. The positions of the hydrogen atoms on the carbon atoms were calculated theoretically. In the course of structural checks for compounds **1**–**3**, we found that some none-H atoms met ADP and NPD problems. In order to avoid them, a restraint comment of "isor" was used to refine the non-H atoms with such problems, which led to relative high restraint values: 270 for **1**, 180 for **2** and 228 for **3**, but this cannot be totally avoid considering about the quality of the data. As for **1**, "isor" was used to refine all the oxygen atoms of PMo_{12} polyanion. As for **2**, the restraint refined atoms with "isor" are as follows: N2, N5, B1, C1, C2, C3, C6, C8, C9, C11, C14 and all the oxygen atoms of BW_{12} polyanion. Besides, another restraint comment of "simu" was used to refine the four disordered oxygen atoms around B1 with very low thermal parameters. The detail is as follows: simu 0.02 0.02 3.8 O1 O4 O8 O11. As for **3**, N1, N3, N6, All oxygen atoms of W_{12} polyanion and all carbon atoms were refined with "isor". "omit 0 51.5" was used to omit the weak reflections above 51.5 degree. Crystallographic data are given in Table 1. Selected bond lengths and angles of the compounds are listed in Table S1.

2.5. Catalytic reaction

In a typical process, the powder of 50 mg compound **1** was dispersed into a 100 mL RhB aqueous solution with the initial concentration of 1.0×10^{-5} mol/L (C_0). Before irradiation, the system was magnetically stirred in the dark for 30 min to ensure

Table 1
Crystal data and structure refinements for Compounds **1**–**3**.

Compound	**1**	**2**	**3**
Empirical formula	$C_{24}H_{25}ClCu_5N_{12}O_{40}PMo_{12}$	$C_{28}H_{28}Ag_5N_{14}O_{40}BW_{12}$	$C_{24}H_{35}Cu_5N_{12}O_{44}W_{12}$
Mr	2656.94	3956.82	3719.39
Temp. (K)	293(2)	293(2)	293(2)
Crystal system	Triclinic	Monoclinic	Triclinic
Space group	*P*-1	*C*2/c	*P*-1
a/Å	11.691(5)	23.353(3)	11.810(5)
b/Å	13.492(5)	20.537(9)	12.377(5)
c/Å	20.615(5)	12.622(6)	12.511(5)
α/°	89.274(5)	90	61.757(5)
β/°	76.749(5)	98.320(3)	71.809(5)
γ/°	66.931(5)	90	70.559(5)
V/Å^3	2901(2)	5990(3)	1492(1)
Z	2	4	1
D_{Calc}/g cm^{-3}	3.040	4.387	4.126
μ(Mo *Kα*)/mm^{-1}	4.468	24.634	24.859
F(0 0 0)	2506.0	6968.0	1637.0
Final R_1[a], wR_2[b] [$I > 2\sigma(I)$]	0.0808 0.2162	0.0860 0.2306	0.0981 0.3046
Goodness of fit on F^2	0.973	1.179	1.185

[a] $R_1 = \sum \| F_o | - | F_c \| / \sum | F_o |$.
[b] $wR_2 = \{\sum [w(F_o^2 - F_c^2)^2] / \sum [w(F_o^2)^2]\}^{1/2}$.

the establishment of adsorption equilibrium. The solution was then surrounded by two 4 W UV lamps with λ_{max}=365 nm. Every certain time interval, 3 mL aliquot was sampled and then centrifuged to remove the particles of catalyst. The RhB concentration (C) was determined by measuring the maximum absorbance at 554 nm as a function of irradiation time using a 756 CRT UV–vis spectrophotometer. In a similar manner, the photocatalytic activities of compounds **2** and **3** were made with compound **1**.

3. Results and discussion

3.1. Synthesis

Compounds **1**–**3** were synthesized under hydrothermal conditions by situ self-assembly process containing Cu/Ag sources and pz molecules, but different starting materials which contribute to form different Keggin ions. Bond valence sum calculations [53] show that: all W atoms in **2** and **3** are in the VI+ oxidation state; two Mo atoms are in the V+ oxidation state while other Mo atoms are in the VI+ oxidation state in **1**; all Cu atoms in compounds **1** and **3** are in the I+ oxidation state, further confirmed by XPS spectra, charge balance, coordination environments and crystal color. The changes of $Cu^{II} \rightarrow Cu^{I}$ and $Mo^{VI+} \rightarrow Mo^{V+}$ may be due to the reducibility of pz organic molecules, which is often observed in the N-donor ligand containing system under hydrothermal conditions [42,54]. Similar to the case of $[Ag_2(3atrz)_2]_2[(HPMo^{VI}_{10}Mo^{V}_{2}O_{40})]$ [42], to balance the charge of the compound, a proton is added and then compound **1** is formulated as $[Cu^{I}_{5}(pz)_6Cl][HPMo^{VI}_{10}Mo^{V}_{2}O_{40}]$. For compound **3**, an additional proton was assigned as an external countercation of α-metatungstate$[H_2W_{12}O_{40}]^{6-}$, so compound **3** was formulated as $[Cu^{I}_{5}(pz)_6H(H_2W_{12}O_{40})] \cdot 4H_2O$ [55].

3.2. Structure description

3.2.1. Structure description of compound *1*

Single X-ray structural analysis reveals that compound **1** is constructed from a coordination complex $[Cu^{I}_{5}(pz)_6Cl]^{4n+}_{n}$ and incorporating $[HPMo^{VI}_{10}Mo^{V}_{2}O_{40}]^{4n-}_{n}$ anions.

In the framework, there are five distinct Cu centers: Cu1 ion adopts a slightly distorted four-coordinated tetrahedron shape, achieved by one N atom from one pz ligand, one Cl atom and two O atoms from two PMo_{12} anions. Cu2 ion, Cu4 ion and Cu5 ion are all four-coordinated in a tetrahedron mode: Cu2 ion is coordinated by three N atoms from three pz molecules and one Cl atom; Cu4 ion is coordinated by two N atoms from two pz ligands, one Cl atom and one O atom from one PMo_{12} anion; Cu5 ion is coordinated by three N atoms from pz molecules and one O atom from one PMo_{12} anion. Cu3 ion shows an almost plane triangle mode, three-coordinated by three N atoms from three pz ligands. The Cl atom bridges Cu1, Cu2 and Cu4 ions to form a Cu_3–Cl cluster (Fig. 1(a)). All pz ligands act as bi-dentate linkers to connect the Cu_3–Cl cluster, Cu3 and Cu5 ions to form a Cl-bridged Cu–pz–Cl double layer, seen from the *b* axis (Fig. 1(b)). The bond distances of Cu–N and Cu–Cl are in the range of 1.912(0)–2.034(2) and 2.147(0)–2.519(1) Å, respectively. The Cu_3–Cl cluster acts as a hexa-dentate ligand linking three Cu3 ions and three Cu5 ions. Both Cu3 and Cu5 serve as three-connected nodes bridging three Cu_3–Cl clusters and locate up and down separately around the Cu_3–Cl cluster. If considering the Cu_3-Cl cluster as a connection node, a (3,3,6)-connected topological structure of $(4^3)(4^3)(4^6 \cdot 6^6 \cdot 8^3)$ is formed (Fig. 1(c)). Noticeably, there exist two kinds of cage-like pores in the double layer along the *b* axis: A is a hexagon unit built by pz ligands and six Cu^{I} ions with the dimensions of ca. 13.586 × 13.378 Å; B is a decagon unit constructed from pz ligands, two Cl bridging atoms and eight Cu^{I} ions with the windows of ca. 13.993 × 16.699 Å (corresponding the shortest intracage Cu…Cu distances). Such phenomenon is uncommon in the Cl-bridged metal-organic frameworks [38–39,56–57].

Another interesting feature for compound **1** lies in the existence of two kinds of PMo_{12} anions locating between the metal-organic double-layers viewed from the *a* axis (Fig. 2(a)). The two kinds of PMo_{12} anions exhibit distinct coordination fashions: one acts as a bi-dentate ligand coordinating with two Cu5 atoms through Cu–O bonds [Cu1–O5 = 2 × 2.475(1) Å] (Fig. 2(b)), while the other acts as a hexa-dentate ligand linking four Cu1 atoms and two Cu4 atoms and then connect each other to a POM–Cu chain through Cu–O interactions [Cu1–O018 = 2 × 2.529 Å, Cu4–O019 = 2 × 2.136 Å, Cu1–O07 = 2 × 2.538 Å] (Fig. 2(c)). So the neighboring double layers are connected by two kinds of PMo_{12} anions through the above Cu–O interactions, forming a 3D POM-incorporated framework.

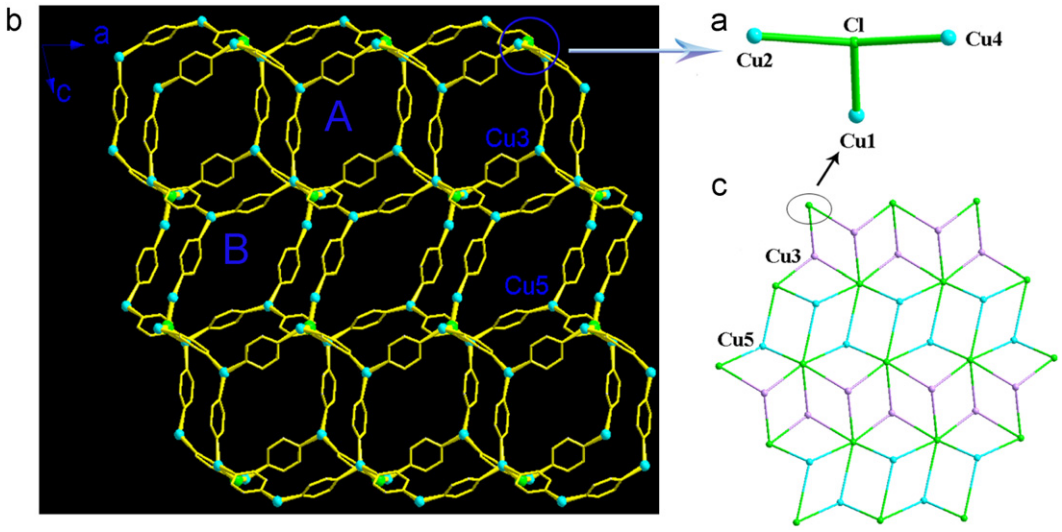

Fig. 1. (a) View of the Cu_3–Cl cluster bridged by Cl atom. (b) The Cu–pz–Cl double layer in compound **1**. (c) The topological view of the double layer (Cu3, lavender; Cu5, blue; Cu_3–Cl cluster, green). (For interpretation of the references to color in this figure legend, the reader is referred to the web version of this article.)

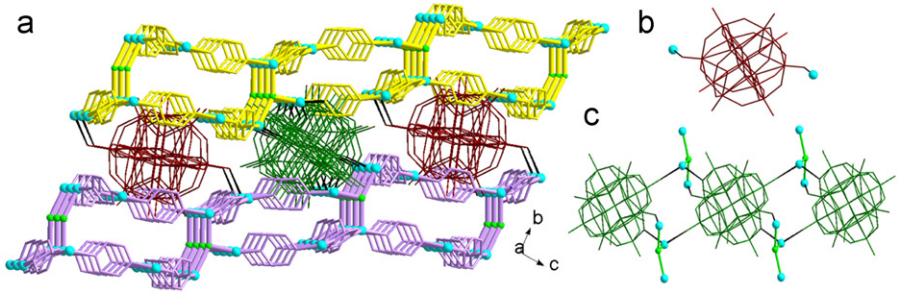

Fig. 2. (a) View of the location of PMo_{12} anions in compound **1** (the black bonds represent Cu…O interactions). (b) The bi-dentate coordination mode of PMo_{12} anion. (c) The hexa-dentate coordination mode of PMo_{12} anion.

3.2.2. *Structure description of compound* ***2***

Single X-ray structural analysis reveals that the structure of **2** is constructed from a coordination complex $[Ag^{I}_{5}(pz)_7]^{5n+}_{n}$ and encapsulating $[BW_{12}O_{40}]^{5n-}_{n}$ anions.

In the framework, there exist four crystallographically unique Ag ions: Ag1 ion is three-coordinated in a plane triangle mode, achieved by three N atoms from three pz ligands. Ag2 ion adopts a distorted octahedral geometry, coordinated by four N atoms from four pz ligands and two O atoms from two BW_{12} anions. Ag3 ion is coordinated by two N atoms from two pz ligands and two O atoms from two BW_{12} anions, forming a slightly distorted tetrahedron shape. Ag4 ion exhibits a trigonal biyramid geometry, five-coordinated by three N atoms of three pz ligands and two O atoms from two BW_{12} anions. The pz ligands as linear bridging linkers alternately connect Ag2, Ag3 and Ag4 ions to form a curve-like Ag–pz chain (Fig. 3(a)). Then adjacent chains are further connected by additional pz ligands as pillars, forming a 2D layer through Ag2–N1 and Ag4–N3 bonds, seen from the *b* and *c* axes (Ag2–N1 = 2.473(2) and Ag4–N3 = 2.306 Å; Figs. 3(b) and (c)). Interestingly, there exists a deca-nuclear metallamacrocycle composed of $Ag_{10}(pz)_{10}$ in the layer.

Further, the pz ligands bridge Ag1 ions to form a wave-like chain. Then the Ag1 wave-like chains connect adjacent layers through Ag1–N bonds to form a 3D Ag–pz framework [Ag1–N2 = 2.259(1) Å], seen from the *b* axis. It represents the first 3D *M*–pz framework up to now (Fig. 4) [45–50]. The overall framework presents parallelogram-like voids with the dimension of ca. 12.712 × 16.188 Å (corresponding the shortest Ag…Ag distances), into which *a*-Keggin type BW_{12} anions located and coordinated with eight Ag ions through Ag–O interactions (Ag2–O21 = 2 × 2.814(1), Ag3–O20 = 2 × 2.550(1), Ag3–O19 = 2 × 2.455(2) and Ag4–O18 = 2 × 2.694(3) Å; Fig. 5).

3.2.3. *Structure description of compound* ***3***

Single X-ray structural analysis reveals that the structure of **3** is constructed from a coordination complex $[Cu^{I}_{5}(pz)_6]^{5n+}_{n}$ and incorporating $[H(H_2W_{12}O_{40})]^{5n-}_{n}$ anions.

In compound **3**, there exist three crystallographically unique Cu^{I} ions: Cu1 and Cu3 ions are both four-coordinated in a tetrahedron mode: Cu1 is coordinated by three N atoms from pz ligands and one O atom from one W_{12} anion; Cu3 is coordinated by two N atoms from two pz ligands and two water molecules (Cu3–Ow1 = 2.193(1) and Cu3–Ow2 = 2.100(1) Å). Cu2 ion shows an octahedral geometry, six-coordinated by two N atoms from pz ligands and four O atoms from two W_{12} anions. All bond distances of Cu–N are in the range of 1.907(1)–2.025(2) Å.

The basic metal-organic coordination framework is Cu–pz cationic layer contributed by the above three kinds of Cu ions and bridged pz ligands. Noticeably, there exists large cucurbit-like pores composed of 12-nuclear metallamacrocycle $Cu_{12}(pz)_{12}$ in the layer. The dimension of half of a cucurbit is ca. 12.550 × 14.531 Å (corresponding the shortest Cu…Cu distances) (Fig. 6(a)). Further, W_{12} Keggin anions act as templates locating in

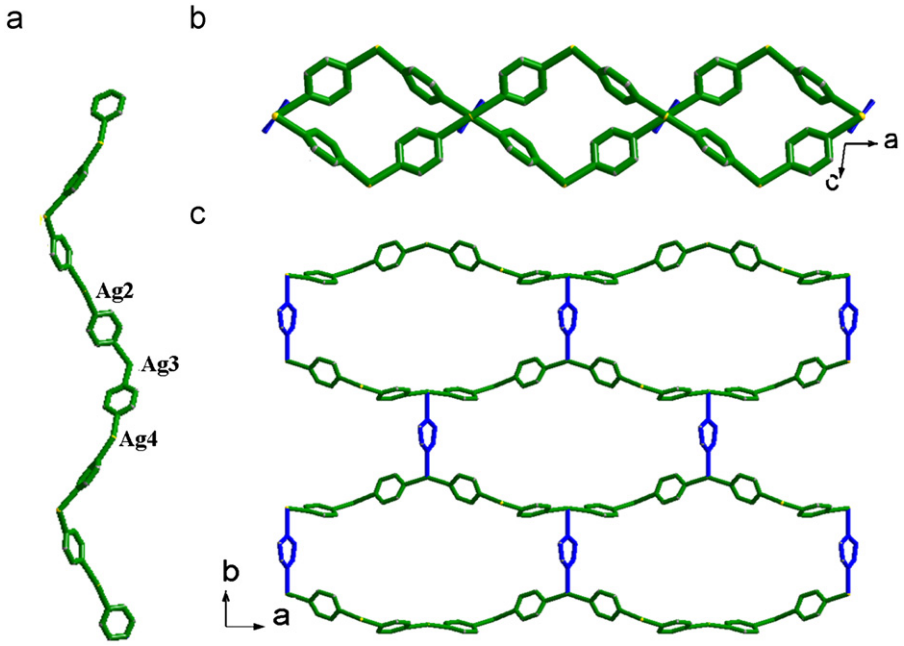

Fig. 3. (a) View of the Ag–pz curve-like chains in compound **2**. (b) The 2D layer along the *b* (b) and *c* (c) axes.

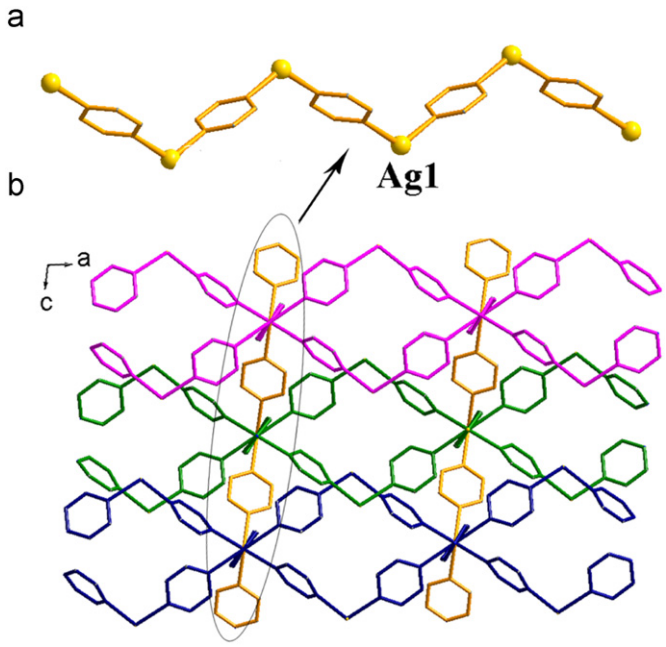

Fig. 4. (a) View of the Ag1 wave-like chain and (b) the adjacent layers connected by the wave-like chain along the *b* axis.

the space between the Cu–pz layers, and then the adjacent chiral Cu–pz sheets are packed to a 3D POM-contained hybrid through weak Cu…O interactions between W_{12} anions and Cu ions (Cu1…O19=2.851(1), Cu2…O15=2.786(1) and Cu2…O11=2.830(1) Å; Fig. 6(b)).

3.3. *Influence of Keggin ions on the structures of compounds **1** and **3***

When comparing compounds **1** and **3**, we found that the two compounds have similar Cu^{I}–pz components but different Keggin clusters: $[HPMo^{VI}_{10}Mo^{V}_{2}O_{40}]^{4-}$ in **1** and $[H(H_2W_{12}O_{40})]^{5-}$ in **3** (Fig. 7). The structural differences could be contributed to three factors: (1) the charge of polyanion; (2) the size of polyanion and (3) the intrinsic nature of Mo and W. First, the Keggin ions of compound **3** have a five charge and five Cu cations participate in the formation of a 2D layer PCP. In contrast, in compound **1**, Keggin cluster has a four charge, to balance the charge, an addition Cl anion participates in the formation of PCP. Thus, a Cl-bridged Cu–pz–Cl double layer is formed, which is built from $[Cu^{I}_{5}(pz)_6Cl]^{4+}$ coordination complex. Second, the sizes of Keggin anions of compounds **1** and **3** are 10.44×10.36 and 10.46×10.43 Å, respectively. They are almost the same and the influence of Keggin anions' size can be excluded. Last, the different intrinsic nature of Mo and W in the two Keggin anions assists the charge of polyanions to influence the final structures. Overall, the charge of Keggin anions presents primary influence on the structures of **1** and **3**. Their structural relations show that the proper choice of Keggin POM is important for the structural properties of PCPs.

3.4. *FT-IR spectra and XRD patterns*

The IR spectra of compounds **1**–**3** are shown in Fig. S1. The characteristic peaks for Keggin anions are assigned as follows: 1060 cm^{-1} in **1**, ascribed to the ν_{as}(P–O_a); 953 cm^{-1} in **1**, 995 and 943 cm^{-1} in **2**, and 949 cm^{-1} in **3**, to the ν_{as}(M–O_d); 866 cm^{-1} in **1**, 889 cm^{-1} in **2** and 895 cm^{-1} in **3**, to the ν_{as}(M–O_b–M); 779 cm^{-1} in **1**, 822 cm^{-1} in **2** and 798 cm^{-1} in **3**, to the ν_{as}(*M*–O_c–*M*) (*M*=Mo, for **1**; W, for **2** and **3**) [58]. In comparison with the corresponding native Keggin POMs, there are some slight changes in peak position, perhaps due to the weak coordination interactions between the POMs and the metal-organic frameworks [59]. The peak at 3420 cm^{-1} in **3** is associated with the water molecules. The characteristic peaks Bonds in the region of 1400–1650 cm^{-1} for **1**, 1050–1650 cm^{-1} for **2** and 1110–1650 cm^{-1} for **3** could be regarded as the characteristics of the pz molecules.

As shown in Fig. S2, the simulative and experimental powder X-ray diffraction patterns of **1**–**3** are coincident well, which confirms the purities for as-synthesized compounds. The intensities of the experimental XRPD patterns are a little weak, due to

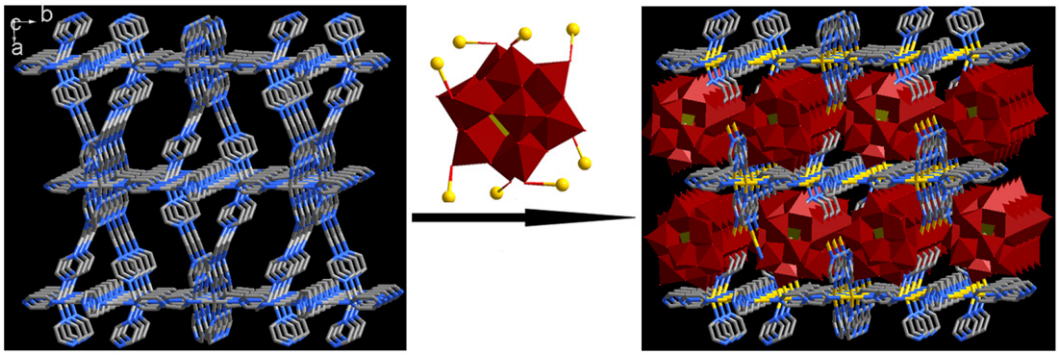

Fig. 5. View of the BW_{12} anions immobilized into the parallelogram-like voids of the 3D Ag–pz framework.

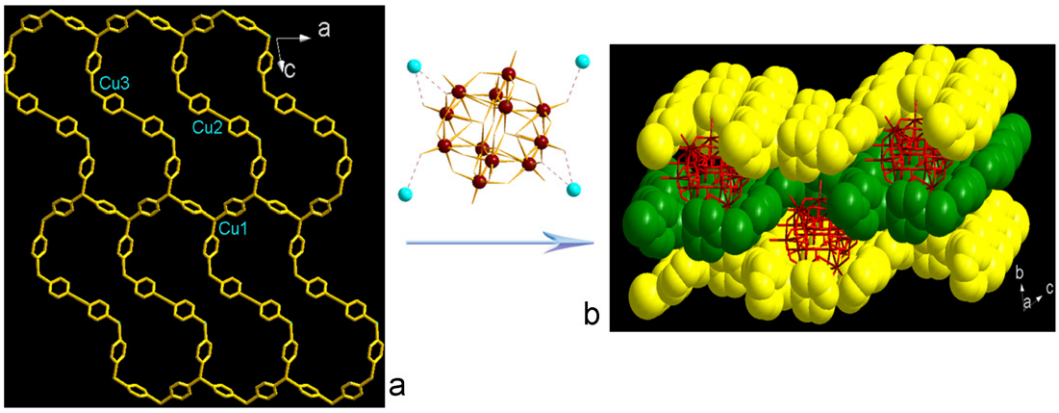

Fig. 6. (a) View of the 2D layer with cucurbit-like pores in compound **3**. (b) The packing style of adjacent layers and the location of W_{12} anions in compound **3**.

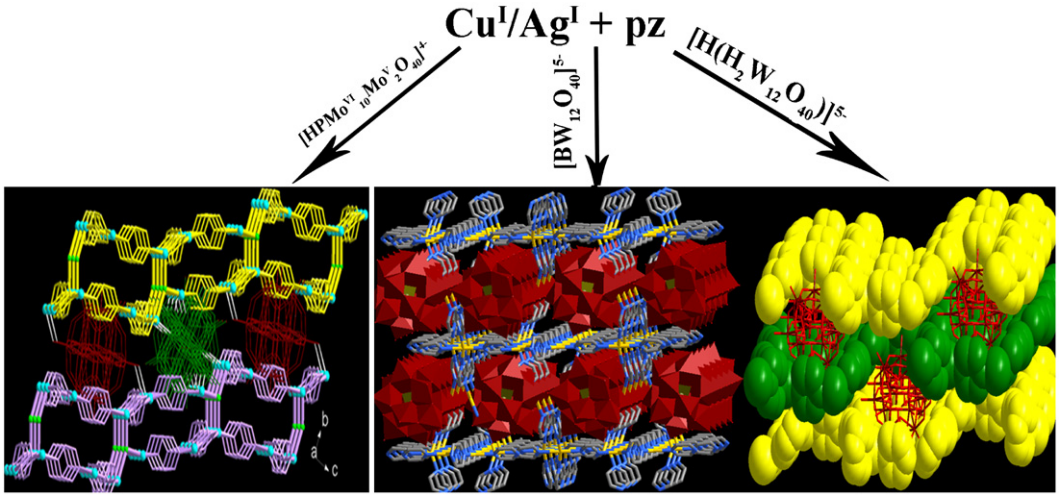

Fig. 7. Summary of the formation of the three PCPs templated by different Keggin ions.

the preferred orientation of the powders and the instrumental limitations.

3.5. XPS spectra

As is shown in Fig. S3, the XPS spectra show two peaks at 932.1 and 952.1 eV for **1** and 932.4 and 952.3 eV for **3**, attributed to $Cu^{+}(2p_{3/2})$ and $Cu^{+}(2p_{1/2})$[25]; two overlapped peaks at 232.3 and 231.5 eV for **1**, attributed to Mo^{6+} and Mo^{5+}, respectively, while a peak at 35.8 and 37.9 eV for **3** are attributed to W^{6+} [60–61]. All these results further confirm the valence sum calculations and the structural analyses.

3.6. Thermal analyses

From the TG curves (Fig. S4), it can be seen that all the three compounds show one step weight loss. The weight losses of 15.11% (calc 18.07%) in the temperature range of 239–410 °C for compound **1** and 18.36% (calc 14.15%) in the temperature range of 233–318 °C for compound **2**, are ascribed to the release of pz ligands. For compound **3**, the weight loss of 16.56% (calc 15.16%) in the temperature range of 101–214 °C corresponds to the loss of coordinated water molecules and decomposition of pz ligands. Given a comparison of the thermal behaviors for compounds **1**–**3**, we can find that the starting temperature of weight losses for **1**

(239 °C) and **2** (233 °C) are higher than **3** (101 °C). This would be reasonably explained by their structural features. The metal-organic moieties in compounds **1** and **2** are 2D double layer and 3D covalently linked framework, respectively. However, in compound **3**, the basic framework is a single Cu–pz layer, which may contribute to a lower thermal stability than the double layer and 3D framework in compounds **1** and **2**. What's more, the coordination interactions between the POMs and the metal-organic moieties exercise another important impact on the case. The average *M*…O (*M*=Cu for **1** and **3**; Ag for **2**) interactions in **3** is about 2.8 Å, which is obviously weaker than approximate 2.5 Å in **1** and **2**.

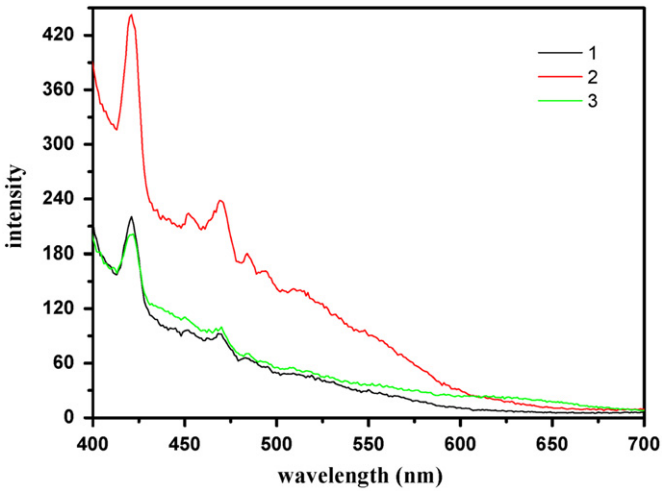

Fig. 8. The solid-state emission spectra of compounds **1**–**3** at room temperature (the excitation wavelength is 370 nm for compounds **1**–**3**).

3.7. Photoluminescent properties

Luminescent compounds are of great interest currently owing to their various applications in chemical sensors, photochemistry, and electroluminescent display [62–64]. The photoluminescent properties of compounds **1**–**3** were studied at room temperature (Fig. 8). It can be observed that the maximum emission wavelength located at 421 nm for **1**, 421 nm for **2** and 422 nm for **3** with the excitation wavelength of 370 nm, which are similar to the emission band of pz ligands with a maximum wavelength of 410 nm (λ_{ex}=346 nm) [65]. It suggests that the luminescence of **1**–**3** mainly originates from ligand-to-metal charge transfer and/or the intraligand ($\pi^* \rightarrow \pi$) fluorescent emission [66].

3.8. Cyclic voltammetry

The electrochemical behaviors of **1**, **2** and **3**-modified carbon paste electrodes (**1**, **2** and **3**-CPE) at different scan rates were investigated in 1 mol L^{-1} H_2SO_4 aqueous solution (Fig. S5). Three pairs of reversible redox peaks (I–I′, II–II′, III–III′) for **1** in the potential range from +800 to −300 mV are observed. The mean peak potentials ($E_{1/2}$=(E_{pa}+E_{pc})/2) of them are +405 mV (I–I′), +112 mV (II–II′), −83 mV (III–III′) (scan rate: 120 mV s^{-1}), respectively. Redox peaks I–I′, II–II′ and III–III′ correspond to three consecutive two-electron processes of Mo centers [39,67].

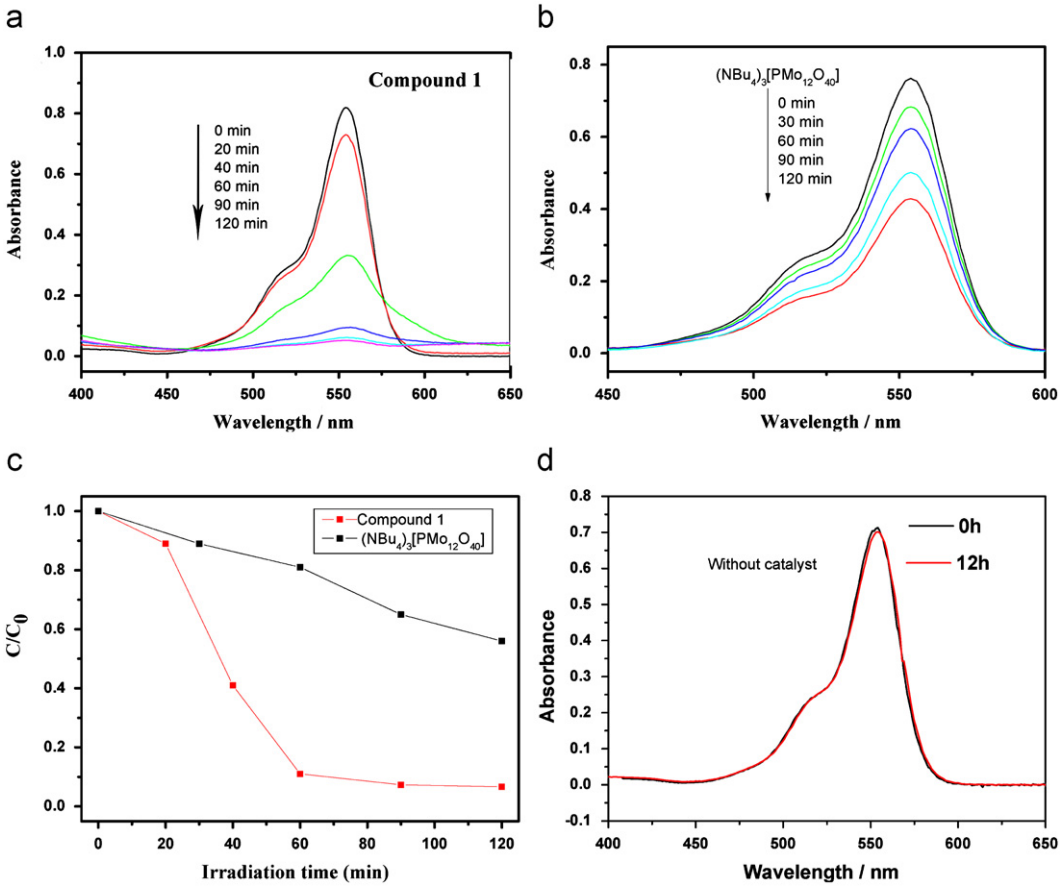

Fig. 9. Temporal UV–vis adsorption changes observed for RhB solutions as a function of UV light irradiation time: (a) in the presence of compound **1** as catalyst; (b) molybdophosphate as catalyst. (c) Time dependence of RhB concentration over compound **1** and molybdophosphate. (d) UV–vis adsorption changes observed for RhB solution without any catalyst.

However, the expected oxidation peak of copper centers is not observed in the scan range of +800 and −300 mV, perhaps due to the overlap of the Mo^{VI}/Mo^{V} redox peak. This phenomenon is similar to the previous case [39]. In the potential range of +600 to −800 mV for **2**-CPE, there exists two reversible redox peaks II–II′ and III–III′ with mean peak potentials at −509 mV (II–II′), −652 mV (III–III′) (scan rate: 120 mV s^{-1}), which can be ascribed to the redox process of W centers [68]. In addition, the irreversible anodic peak I with peak potential of +424 mV is assigned to the oxidations of silver centers [69]. For **3**-CPE, two redox peaks II–II′ and III–III′ are also observed in the potential range of +600 to −800 mV. The mean peak potentials of them are +16 mV (II–II′), −556 mV (III–III′) (scan rate: 120 mV s^{-1}), corresponding to the redox activity of W centers [70]. Another irreversible anodic peak I with peak potential of +359 mV is assigned to the oxidations of copper centers. Furthermore, when the scan rate was increased for **1**, **2** and **3**-CPE, the peak potentials changed gradually: the cathodic peak potentials shifted to the negative direction and the corresponding anodic peak potentials to the positive direction. Namely, the peak-to-peak separation between the corresponding cathodic and anodic peaks increased, but the mean peak potentials did not change on the whole.

3.9. Photocatalytic activity

To investigate the photocatalytic activities of the three compounds as catalysts, the photodecomposition of RhB is evaluated under UV light irradiation. The photocatalytic activities are monitored by UV–vis measurements at certain time intervals. As shown in Fig. 9, after irradiation compound **1** for 120 min, the photocatalytic decomposition rate, defined as $1—C/C_0$, is 99.93%. During the degradation process with compound **1** as catalyst, the color of RhB solution changed from the rose color, aubergine to lavender, and finally came to nearly colorless (Fig. S6), while it seems no change without any catalyst after irradiating for 12 h or in the dark for 24 h. In contrast, the photocatalytic decomposition rate using insoluble molybdophosphate $(NBu_4)_3[PMo_{12}O_{40}]$ as catalyst is just 43.75% after UV light irradiation of 120 min (Fig. 9(b) and (c)), which illustrates that the formation of organic—inorganic hybrid compounds based on metal-pyrazine coordination polymers and Keggin polyoxometalates could improve the photocatalytic performance of the molybdophosphates. The enhanced photocatalytic property may be arisen from the $[Cu^{I}_5(pz)_6Cl]^{4n+}_n$ complex acting as photosensitizer under UV light, which promotes transition of electrons to PMo_{12} anions [3]. Irradiating compound **2** for 6 h, the photocatalytic decomposition rate just goes up to 33% (Fig. S7). For compound **3**, after irradiation for 4 h, no decomposition of RhB was observed. It indicates that compound **1** presents excellent degradation activity and may be a potential photocatalyst to decompose some organic dye. This phenomenon may be attributed to the stronger oxidation ability of Mo center than W center.

4. Conclusions

In this paper, three different Cu^{I}/Ag–pz porous coordination polymers (PCPs) immobilizing different Keggin POM templates have been obtained. The successful syntheses of the compounds demonstrated that the structural properties of PCPs could be influenced by different Keggin templates. Compound **1** presents a Cu–pz–Cl double layer templated by PMo_{12} anions, compound **2** shows a 3D Ag–pz framework incorporating BW_{12} templates while a W_{12}-templated layer framework forms in compound **3**. Further, Compound **1** exhibits an enhanced photocatalytic activity than molybdophosphate, which could be identified as a potential photocatalyst to decompose some organic dye.

Supplementary materials

Crystallographic data for the structures have been deposited with Cambridge Crystallographic Data Center with CCDC numbers: 773935 for **1**, 773936 for **2** and 773937 for **3**. Electronic Supplementary Information (ESI) available: Crystallographic data in CIF format; Tables including selected bond length and bond angles for compounds **1**–**3**; IR, TG, XRD, XPS and cyclic voltammograms of **1**–**3** in PDF format.

Acknowledgments

This work is financially supported by the National Natural Science Foundation of China (21071029) and the Analysis and Testing Foundation of Northeast Normal University.

Appendix A. Supplementary material

Supplementary data associated with this article can be found in the online version at doi:10.1016/j.jssc.2011.03.030.

References

[1] C.Y. Sun, S.X. Liu, D.D. Liang, K.Z. Shao, Y.H. Ren, Z.M. Su, J. Am. Chem. Soc. 131 (2009) 1883.
[2] S.Y. Gao, R. Cao, J. Lu, G.L. Li, Y.F. Li, H.X. Yang, J. Mater. Chem. 19 (2009) 4157.
[3] H.X. Yang, T.F. Liu, M.N. Cao, H.F. Li, S.Y. Gao, R. Cao, Chem. Commun. 46 (2010) 2429.
[4] Y.L. Zhong, W.B.W. Ng, J.X. Yang, K.P. Loh, J. Am. Chem. Soc. 131 (2009) 18293.
[5] E. Coronado, S. Curreli, C. Gimenez-Saiz, C.J. Gomez-Garcıa, A. Alberola, E. Canadell, Inorg. Chem. 48 (2009) 11314.
[6] M.A. AlDamen, S. Cardona-Serra, J.M. Clemente-Juan, E. Coronado, A. Gaita-Arino, C. Martí-Gastaldo, F. Luis, O. Montero, Inorg. Chem. 48 (2009) 3467.
[7] S.T. Zheng, G.Y. Yang, Dalton Trans. 39 (2010) 700.
[8] Z.L. Wang, R.L. Zhang, Y. Ma, L. Zheng, A.D. Peng, H.B. Fu, J.N. Yao, J. Mater. Chem. 20 (2010) 1107.
[9] B. Qin, H.Y. Chen, H. Liang, L. Fu, X.F. Liu, X.H. Qiu, S.Q. Liu, R. Song, Z.Y. Tang, J. Am. Chem. Soc. 132 (2010) 2886.
[10] C.G. Liu, W. Guan, P. Song, Z.M. Su, C. Yao, E.B. Wang, Inorg. Chem. 48 (2009) 8115.
[11] A. Proust, R. Thouvenot, P. Gouzerh, Chem. Commun. (2008) 1837.
[12] Y. Guo, C. Hu, J. Mol. Catal. A 262 (2007) 136.
[13] B.J.S. Johnson, A. Stein, Inorg. Chem. 40 (2001) 801.
[14] R.J. Errington, S.S. Petkar, B.R. Horrocks, A. Houlton, L.H. Lie, S.N. Patole, Angew. Chem. Int. Ed. 44 (2005) 1254.
[15] W. Kaleta, K. Nowinska, Chem. Commun. (2001) 535.
[16] M.V. Vasylyev, R. Neumann, J. Am. Chem. Soc. 126 (2004) 884.
[17] O.A. Kholdeeva, M.P. Vanina, M.N. Timofeeva, R.I. Maksimovskaya, T.A. Trubitsina, M.S. Melgunov, E.B. Burgina, J. Mrowiec-Bialon, A.B.C. Jarzebski, L. Hill, J. Catal. 226 (2004) 363.
[18] J. Kasai, Y. Nakagawa, S. Uchida, K. Yamaguchi, N. Mizuno, Chem. Eur. J. 12 (2006) 4176.
[19] C.G. Silva, A. Corma, H. Garcıa, J. Mater. Chem. 20 (2010) 3141.
[20] M. Savonnet, D. Bazer-Bachi, N. Bats, J. Perez-Pellitero, E. Jeanneau, V. Lecocq, C. Pinel, D. Farrusseng, J. Am. Chem. Soc. 132 (2010) 4518.
[21] K.C. Stylianou, R. Heck, S.Y. Chong, J. Bacsa, J.T.A. Jones, Y.Z. Khimyak, D. Bradshaw, M.J. Rosseinsky, J. Am. Chem. Soc. 132 (2010) 4119.
[22] Q. Xu, D.H. Liu, Q.Y. Yang, C.L. Zhong, J.G. Mi, J. Mater. Chem. 20 (2010) 706.
[23] C.Y. Duan, M.L. Wei, D. Guo, C. He, J.Q. Meng, J. Am. Chem. Soc. 132 (2010) 3321.
[24] O.K. Farha, C.D. Malliakas, M.G. Kanatzidis, J.T. Hupp, J. Am. Chem. Soc. 132 (2010) 950.
[25] Z.Y. Gu, X.P. Yan, Angew. Chem. Int. Ed. 49 (2010) 1477.
[26] Z.Q. Wang, K.K. Tanabe, S.M. Cohen, Chem. Eur. J. 16 (2010) 212.
[27] X.L. Wang, H.Y. Lin, Y.F. Bi, B.K. Chen, G.C. Liu, J. Solid State Chem. 181 (2008) 556.
[28] D. Chandra, M.W. Kasture, A. Bhaumik, Microporous Mesoporous Mater. 116 (2008) 204.
[29] P.P. Zhang, J. Peng, H.J. Pang, Y. Chen, M. Zhu, D.D. Wang, M.G. Liu, Y.H. Wang, Solid State Sci. 12 (2010) 1585.

[30] G. Férey, C. Mellot-Draznieks, C. Serre, F. Millange, J. Dutour, S. Surble, I. Margiolaki, Science 309 (2005) 2040.
[31] N.V. Maksimchuk, M.N. Timofeeva, M.S. Melgunov, A.N. Shmakov, Y.A. Chesalov, D.N. Dybtsev, V.P. Fedin, O.A. Kholdeeva, J. Catal. 257 (2008) 315.
[32] R.M. Yu, X.F. Kuang, X.Y. Wu, C.Z. Lu, J.P. Donahueb, Coordination Chem. Rev. 253 (2009) 2872.
[33] M.L. Wei, C. He, Q.Z. Sun, Q.J. Meng, C.Y. Duan, Inorg. Chem. 46 (2007) 5957.
[34] C. Inman, J.M. Knaust, S.W. Keller, Chem. Commun. (2002) 156.
[35] X.Y. Zhao, D.D. Liang, S.X. Liu, C.Y. Sun, R.G. Cao, C.Y. Gao, Y.H. Ren, Z.M. Su, Inorg. Chem. 47 (2008) 7133.
[36] C.H. Li, K.L. Huang, Y.N. Chi, X. Liu, Z.G. Han, L. Shen, C.W. Hu, Inorg. Chem. 48 (2009) 2010.
[37] K. Uehara, K. Kasai, N. Mizuno, Inorg. Chem. 46 (2007) 2563.
[38] L. Yuan, C. Qin, X.L. Wang, E.B. Wang, S. Chang, Eur. J. Inorg. Chem. 31 (2008) 4936.
[39] X.L. Wang, Y.F. Bi, K.B. Chen, H.Y. Lin, G.C. Liu, Inorg. Chem. 47 (2008) 2442.
[40] C.Y. Sun, Y.G. Li, E.B. Wang, D.R. Xiao, H.Y. An, L. Xu, Inorg. Chem. 46 (2007) 1563.
[41] Y.Q. Lan, S.L. Li, X.L. Wang, K.Z. Shao, Z.M. Su, E.B. Wang, Inorg. Chem. 47 (2008) 529.
[42] Q.G. Zhai, X.Y. Wu, S.M. Chen, Z.G. Zhao, C.Z. Lu, Inorg. Chem. 46 (2007) 5046.
[43] A.X. Tian, J. Ying, J. Peng, J.Q. Sha, H.J. Pang, P.P. Zhang, Y. Chen, M. Zhu, Z.M. Su, Inorg. Chem. 48 (2009) 100.
[44] B.X. Dong, J. Peng, C.J. Gomez-García, S. Benmansour, H.Q. Jia, N.H. Hu, Inorg. Chem. 46 (2007) 5933.
[45] X.J. Kong, Y.P. Ren, P.Q. Zheng, Y.X. Long, L.S. Long, R.B. Huang, L.S. Zheng, Inorg. Chem. 45 (2006) 10702.
[46] Y.P. Ren, X.J. Kong, X.Y. Hu, M. Sun, L.S. Long, R.B. Huang, L.S. Zheng, Inorg. Chem. 45 (2006) 4016.
[47] X.T. Zhang, J.M. Dou, P.H. Wei, D.C. Li, B. Li, C.W. Shi, B. Hu, Inorg. Chim. Acta 362 (2009) 3325.
[48] M.I. Khan, E. Yohannes, V.O. Golub, C.J. O'Connor, R.J. Doedens, Chem. Mater. 19 (2007) 4890.
[49] L. Wang, X.P. Sun, M.L. Liu, Y.Q. Gao, W. Gu, X. Liu, J. Clust. Sci. 19 (2008) 531.
[50] F.Y. Cui, X.Y. Ma, C. Li, T. Dong, Y.Z. Gao, Z.G. Han, Y.N. Chi, C.W. Hu, J. Solid State Chem. 183 (2010) 2925.
[51] G.M. Sheldrick, SHELX-97, Program for Crystal Structure Refinement, University of Göttingen, Germany, 1997.
[52] G.M. Sheldrick, SHELXL-97, Program for Crystal Structure Solution, University of Göttingen, Germany, 1997.
[53] I.D. Brown, D. Altermatt, Acta Crystallogr. Sect. B 41 (1985) 244.
[54] X.L. Wang, H.L. Hu, G.C. Liu, H.Y. Lin, A.X. Tian, Chem. Commun. (2010) 6485.
[55] C.R. Sprangers, J.K. Marmon, D.C. Duncan, Inorg. Chem. 45 (2006) 9628.
[56] Y. Wang, D.R. Xiao, L.L. Fan, E.B. Wang, J. Liu, J. Mol. Struct. 843 (2007) 87.
[57] H. Jin, Y.F. Qi, E.B. Wang, Y.G. Li, C. Qin, X.L. Wang, S. Chang, Eur. J. Inorg. Chem. (2006) 4541.
[58] C. Rocchiccioli-Deltcheff, M. Fournier, R. Franck, R. Thouvenot, Inorg. Chem. 22 (1983) 207.
[59] R. Thouvenot, M. Fournier, R. Franck, C. Rocchiccioli-Deltcheff, Inorg. Chem. 23 (1984) 598.
[60] T.A. Patterson, J.C. Carver, D.E. Leyden, D.M. Hercules, J. Phys. Chem. 80 (1976) 1702.
[61] C.D. Wagner, W.M. Riggs, L.E. Davis, J.F. Moulder, G.E. Muilenberg, Handbook of X-ray Photoelectron Spectroscopy, Perkin-Elmer Corp, MI, 1978.
[62] J.E. McGarrah, Y.J. Kim, M. Hissler, R. Eisenberg, Inorg. Chem. 40 (2001) 4510.
[63] Q. Wu, M. Esteghamatian, N.X. Hu, Z. Popovic, G. Enright, Y. Tao, M. D'Iorio, S. Wang, Chem. Mater. 12 (2000) 79.
[64] G.D. Santis, L. Fabbrizzi, M. Licchelli, A. Poggi, A. Taglietti, Angew. Chem. Int. Ed. Engl. 35 (1996) 202.
[65] C. Yang, M.S. Wang, Z.N. Xu, F. Chen, G.N. Liu, G. Xu, G.C. Guo, J.S. Huang, Inorg. Chem. Commun. 13 (2010) 326.
[66] J.H. Luo, M.C. Hong, R.H. Wang, Q. Shi, R. Cao, J.B. Weng, R.Q. Sun, H.H. Zhang, Inorg. Chem. Commun. 6 (2003) 702.
[67] P. Wang, Y. Yuan, Z.B. Han, G.Y. Zhu, J. Mater. Chem. 11 (2001) 549.
[68] S.L. Gao, R. Cao, X. Li, Thin Solid Films 500 (2006) 283.
[69] S. Berchmans, R.G. Nirmal, G. Prabaharan, S. Madhu, V.J. Yegnaraman, Colloid Interface Sci. 303 (2006) 604.
[70] M. Sadakane, E. Steckhan, Chem. Rev. 98 (1998) 219.